Determination of the Protein Backbone Dihedral Angle ψ from a Combination of NMR-Derived Cross-Correlation Spin Relaxation Rates

Daiwen Yang* and Lewis E. Kay*

Contribution from the Protein Engineering Network Centers of Excellence and Departments of Molecular and Medical Genetics, Biochemistry and Chemistry, University of Toronto, Toronto, Ontario, Canada M5S 1A8

Received May 29, 1998. Revised Manuscript Received July 30, 1998

Abstract: A sensitive triple resonance NMR experiment is presented for the measurement of the protein backbone dihedral angle ψ based on cross-correlated spin relaxation between $^{13}C^{\alpha}-^{1}H^{\alpha}$ and $^{15}N-^{1}HN$ dipolar interactions in $^{15}N,^{13}C$-labeled proteins. In general, as many as four ψ values can be consistent with a single cross-correlation rate. However, in many cases, the ambiguity can be significantly reduced (for example, from four to two) when a combination of cross-correlation relaxation rates are employed. This is illustrated by considering rates derived from $^{13}C^{\alpha}-^{1}H^{\alpha}/^{15}N-^{1}HN$ dipolar and from $^{13}C^{\alpha}-^{1}H^{\alpha}$ dipolar/carbonyl chemical shift anisotropy relaxation mechanisms for the proteins ubiquitin and CheY. Using a database of ψ values obtained from high-resolution X-ray structures, it is shown that for values in the range $-50° \leq \psi \leq 40°$ a single ψ can be obtained to high probability.

Introduction

It is now well established that NMR cross-correlated spin relaxation experiments can provide dynamical[1−3] as well as structural information about molecules in solution.[4] In the case of structural studies, Griesinger and co-workers have described a powerful strategy which makes use of cross-correlated spin relaxation to measure the angles between bond vectors which does not require a parametrized Karplus-type relationship.[4] In a demonstration of the utility of the method this group has shown that the cross-correlated spin relaxation rate arising from $^{13}C^{\alpha}-^{1}H^{\alpha}$ (residue *i*) and $^{15}N-^{1}HN$ (residue $i+1$) dipolar interactions, denoted by $\Gamma_{H\alpha C\alpha,HN}$, is related to the peptide dihedral angle ψ. Building on this significant result, Yang et al. have developed an experiment for measuring ψ based on the cross-correlation rate between intraresidue $^{13}C^{\alpha}-^{1}H^{\alpha}$ dipolar and $^{13}C'$ (carbonyl) chemical shift anisotropy (CSA) relaxation mechanisms,[5,6] $\Gamma_{H\alpha C\alpha,C'}$. This experiment offers significant improvements in sensitivity and resolution relative to the original dipole−dipole experiment[4] and has been demonstrated on a system as large as 42 kDa, comprising the 370 residue maltose binding protein and β-cyclodextrin.[6]

A limitation associated with the use of cross-correlated spin relaxation to measure angles relates to the multiplicity of values which are possible from the measurement of only a single relaxation rate. For example, in the worst case, four different ψ values are possible from measurement of either (but not both) $^{13}C^{\alpha}-^{1}H^{\alpha}$ dipolar/$^{15}N-^{1}HN$ dipolar or $^{13}C^{\alpha}-^{1}H^{\alpha}$ dipolar/$^{13}C'$ CSA cross-correlation rates. It is clear, however, that by combining measurements from both methods the possibilities can be reduced considerably. With this in mind we present a new experiment for measuring $^{13}C^{\alpha}-^{1}H^{\alpha}$ dipolar/$^{15}N-^{1}HN$ dipolar cross-correlation which offers substantial improvements in both sensitivity and resolution relative to the original scheme.[4] Using data recorded on two proteins, ubiquitin and CheY, we show that a combination of both $\Gamma_{H\alpha C\alpha,HN}$ and $\Gamma_{H\alpha C\alpha,C'}$ cross-correlation rates and database information relating to the preference of ψ values in proteins often leads to a reduction in the number of possible ψ values by a factor of 2 and in many cases the ambiguity in ψ can be eliminated altogether.

Materials and Methods

$^{15}N,^{13}C$-labeled samples of ubiquitin and CheY were provided by Professors J. Wand (SUNY Buffalo) and R. Dahlquist (University of Oregon), respectively. Sample conditions were 2 mM protein, 50 mM potassium phosphate, pH 5.0, and 90% H_2O/10% D_2O for ubiquitin and 1.7 mM protein, 5 mM $MgCl_2$, pH 6.8, and 90% H_2O/10% D_2O for CheY. All spectra were recorded at 30 °C on a Varian UNITY+ 500-MHz spectrometer equipped with a pulsed field gradient unit and a triple resonance probe head. Data sets of $44 \times 19 \times 512$ and $32 \times 25 \times 512$ complex points were collected corresponding to acquisition times of 23.1, 16.9, and 64 ms and 15.1, 23.7, and 64 ms for ubiquitin and CheY, respectively. The delay between points a and b in Figure 1 ($A + B + C + D + pwHN = T_C$, where pwHN is the pulse width of the selective ^{1}HN pulse) was set to 26 and 18 ms for spectra of ubiquitin and CheY, respectively. Relaxation delays of 1 s were used for both data sets corresponding to total acquisition times of 7.5 and 14.5 h for each 3D data set for ubiquitin and CheY, respectively. As described in detail below multiplet components are separated into individual 3D data sets on the basis of the ^{1}HN spin state, thus doubling the resolution without any sacrifice in sensitivity. This is achieved by recording in an interleaved manner two 3D matrices[7,8] [each of 7.5 h (ubiquitin) or 14.5 h (CheY)] and adding or subtracting the resulting

(1) Werbelow, L. G.; Grant, D. M. *Adv. Magn. Reson.* **1977**, *9*, 189−299.
(2) Vold, R. L.; Vold, R. R. *Prog. NMR Spectrosc.* **1978**, *12*, 79−133.
(3) Daragan, V. A.; Mayo, K. H. *Biochemistry* **1993**, *32*, 11488−11499.
(4) Reif, B.; Hennig, M.; Griesinger, C. *Science* **1997**, *276*, 1230−1233.
(5) Yang, D.; Konrat, R.; Kay, L. E. *J. Am. Chem. Soc.* **1997**, *119*, 11938−11940.
(6) Yang, D.; Gardner, K. H.; Kay, L. E. *J. Biomol. NMR* **1998**, *11*, 213−220.
(7) Yang, D.; Nagayama, K. *J. Magn. Reson. Ser. A* **1996**, *118*, 117−121.
(8) Sorensen, M. D.; Meissner, A.; Sorensen, O. W. *J. Biomol. NMR* **1997**, *10*, 181−186.

S0002-7863(98)01873-3 CCC: $15.00
Published on Web 09/09/1998

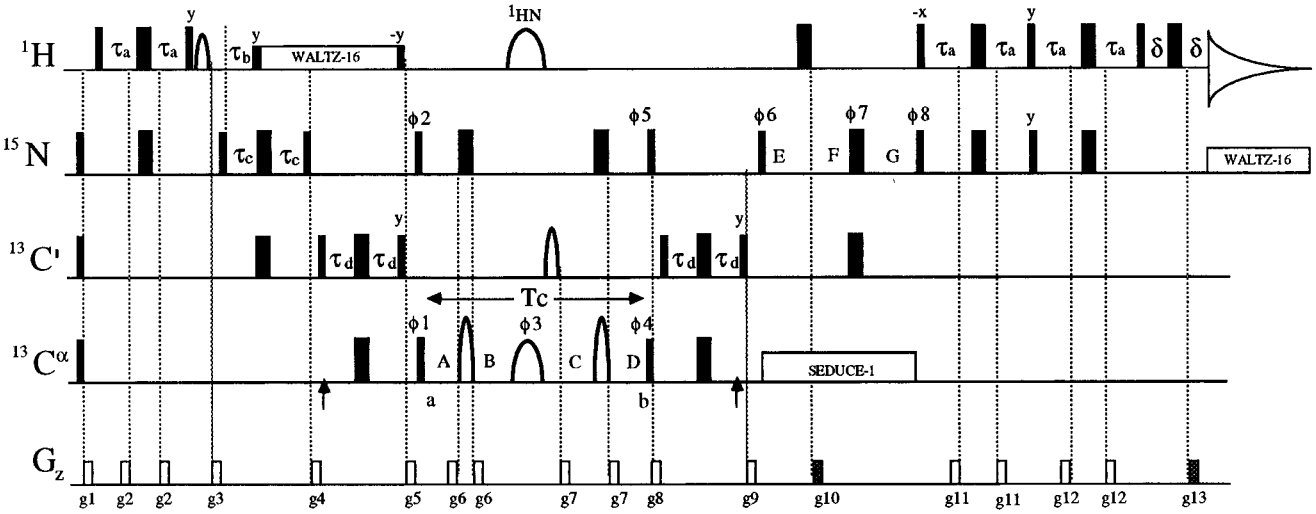

Figure 1. Pulse scheme used to measure the cross-correlation spin relaxation rate derived from $^{13}C^{\alpha}-^{1}H^{\alpha}$ and $^{15}N-^{1}HN$ dipolar interactions. All narrow (wide) pulses are applied with flip angles of 90° (180°) and are along the *x* axis, unless indicated otherwise. The ^{1}H and ^{15}N carriers are positioned at 4.72 ppm (water) and 119 ppm, respectively, while the ^{13}C carrier is set at 176 ppm except for the period extending from points a to b (including $^{13}C^{\alpha}$ pulses of phase ϕ_1 and ϕ_4) where it is at 55 ppm. All proton pulses are applied with as high a field as possible with the exception of the WALTZ-16[26] decoupling elements and the flanking pulses (6 kHz), the 2-ms 90° water flip back pulse and ^{1}HN-selective refocusing pulse (see below). ^{15}N pulses use a 6.2-kHz field, while decoupling during acquisition is achieved with a 1-kHz field. All $^{13}C'$ rectangular pulses and $^{13}C^{\alpha}$ 90° pulses are applied with a field strength of $\Delta/\sqrt{15}$, where Δ is the separation in hertz between the centers of the $^{13}C^{\alpha}$ and $^{13}C'$ chemical shift regions,[27] while $^{13}C^{\alpha}$ 180° rectangular pulses employ a field strength of $\Delta/\sqrt{3}$ (118 ppm phase modulation of the carrier[28,29]). The first (second) $^{13}C^{\alpha}$ 180° rectangular pulse is applied after (before) the $^{13}C'$ 180° pulses, and the positions of the arrows indicate placement of the Bloch−Siegert compensation pulses.[15] The $^{13}C'$ shaped pulse has a G3[30] profile (490 μs, 7.3 kHz peak radiofrequency (rf), 121 ppm phase modulation of the carrier) and is applied immediately after the simultaneous selective ^{1}HN and $^{13}C^{\alpha}$ pulses. All $^{13}C^{\alpha}$-shaped pulses are applied with the RE-BURP[17] profile. The first and third pulses are of duration 400 μs (15.6-kHz peak rf, excitation centered at 50 ppm by 5 ppm phase modulation of the carrier), while the duration of the second pulse is 2 ms (3.1-kHz peak rf, excitation centered at 55 ppm). The ^{1}HN-selective proton-shaped pulse is applied with the RE-BURP profile (2.3 ms, 2.7-kHz peak rf, ≈4 ppm phase modulation of the ^{1}H carrier depending on the center of the HN region). Decoupling of $^{13}C^{\alpha}$ spins during the ^{15}N evolution period is achieved using a 118 ppm modulated WALTZ-16 sequence with the shape of each of the decoupling elements (355.5 μs) given by the SEDUCE-1[31] profile. The pulse widths reported are those used at 500 MHz (^{1}H frequency) and should be adjusted for applications at different fields or to achieve the desired selectivity. Note that the ^{15}N pulse of phase ϕ_2 (ϕ_5) is applied prior to (after) the $^{13}C^{\alpha}$ pulse of phase ϕ_1 (ϕ_4) and a delay of $-$pwca90 $-$ $(2/\pi)$(pwn90) + 0.5(pwHN) is inserted between the pulses, where pwca90 and pwn90 are the durations of the $^{13}C^{\alpha}$ and ^{15}N 90° pulses, respectively, and pwHN is the duration (2.3 ms) of the ^{1}HN-selective ^{1}H pulse. The delays used are $\tau_a = 2.3$ ms, $\tau_b = 5.5$ ms, $\tau_c = 12.4$ ms, $\tau_d = 4.5$ ms, $\delta = 0.5$ ms, $A = (T + t_1)/4$; $B = (T - t_1)/4$, $C = (T + t_1)/4$, $D = (T - t_1)/4$, $E = t_x + t_2/2$, $F = T_N - t_x$, $G = T_N - t_2/2$, $T = 24$ ms for ubiquitin and 16 ms for CheY ($T_C = T$ + pwHN), and $T_N = 12.4$ ms; t_x is set to 2.75 and 0 ms for the $\cos(\pi J_{NH}t_1)$- and $\sin(\pi J_{NH}t_1)$-modulated data sets, respectively. The phase cycling employed for the $\cos(\pi J_{NH}t_1)$-modulated 3D data set is $\phi_1 = (x,-x)$, $\phi_2 = (x,-x)$; $\phi_3 = 2(x)$, $2(y)$, $2(-x)$, $2(-y)$; $\phi_4 = x$; $\phi_5 = x$; $\phi_6 = x$; $\phi_7 = 4(x)$, $4(-x)$; $\phi_8 = x$; rec = $2(x)$, $2(-x)$. The phases ϕ_4, ϕ_5, and ϕ_6 are incremented by 90° for the $\sin(\pi J_{NH}t_1)$-modulated 3D data set. Quadrature detection in F_1 is achieved by States-TPPI[32] of ϕ_1, while quadrature in F_2 employs the enhanced sensitivity pulsed field gradient method,[33,34] where for each value of t_2 separate data sets are recorded for (g_{10}, ϕ_8) and ($-g_{10}$, ϕ_8 + 180°). For each successive t_2 value, ϕ_6 and the phase of the receiver are incremented by 180°. The $\cos(\pi J_{NH}t_1)$- and $\sin(\pi J_{NH}t_1)$-modulated 3D data sets are recorded in an interleaved manner and are added/subtracted to yield 3D data sets separated by the ^{1}HN spin state using in-house written software. The duration and strengths of the gradients are $g_1 = (0.5$ ms, 8 G/cm), $g_2 = (0.5$ ms, 5 G/cm), $g_3 = (1$ ms, 15 G/cm), $g_4 = (1$ ms, 10 G/cm), $g_5 = (1$ ms, 8 G/cm), $g_6 = (0.1$ ms, 20 G/cm), $g_7 = (0.1$ ms, -25 G/cm), $g_8 = (1$ ms, -10 G/cm), $g_9 = (1$ ms, -15 G/cm), $g_{10} = (1.25$ ms, 30 G/cm), $g_{11} = (0.4$ ms, 5 G/cm), $g_{12} = (0.3$ ms, 4 G/cm), and $g_{13} = (0.125$ ms, -29 G/cm). Decoupling is interrupted during application of the gradients.[35]

matrices using in-house written software. All spectra were processed using NMRPipe/NMRDraw[9] as described previously,[5] with doubling of the t_1 and t_2 time domain points achieved using mirror-image linear prediction.[10] The data were analyzed using the CAPP/PIPP[11] suite of programs.

$\Gamma_{H\alpha C\alpha,HN}$ cross-correlation rates were measured from the data as described below, while $\Gamma_{H\alpha C\alpha,C'}$ cross-correlation rates were obtained using a previously published scheme.[6] Values of ψ for both ubiquitin and CheY were extracted from a combination of $\Gamma_{H\alpha C\alpha,HN}$ and $\Gamma_{H\alpha C\alpha,C'}$ cross-correlation rates by minimizing the function

$$\chi^2 = (\Gamma_{H\alpha C\alpha,HN}{}^{cal} - \Gamma_{H\alpha C\alpha,HN}{}^{exp})^2 + (\Gamma_{H\alpha C\alpha,C'}{}^{cal} - \Gamma_{H\alpha C\alpha,C'}{}^{exp})^2 \quad (1)$$

independently for each residue, where the superscripts "cal" and "exp" refer to calculated and experimentally determined cross-correlation rates. An expression for $\Gamma_{H\alpha C\alpha,HN}{}^{cal}$ is given below, while $\Gamma_{H\alpha C\alpha,C'}{}^{cal}$ is defined elsewhere.[5,6] Expression 1 was minimized by dividing the range of ψ values [−180°,180°] into seven intervals, [−180°,−155°], [−155°,−138°], [−138°,−60°], [−60°,18°], [18°,35°], [35°,120°], and [120°,180°], so that multiple minima were not present in any interval in which χ^2 was minimized. χ^2 was minimized independently in each of the seven intervals, and the ψ values with the lowest χ^2 in all of the intervals were selected as solutions. Values of ψ were also obtained exclusively from either $\Gamma_{H\alpha C\alpha,HN}$ or $\Gamma_{H\alpha C\alpha,C'}$ (not both) using a minimization procedure very similar to that described in the case where a combination of both cross-correlation rates was employed. Values of ψ are listed along with values from the X-ray structure in Table 1 for CheY and in Supporting Information for ubiquitin.

Results and Discussion

Description of the Pulse Scheme. Figure 1 illustrates the pulse sequence that has been developed for measuring $\Gamma_{H\alpha C\alpha,HN}$.

(9) Delaglio, F.; Grzesiek, S.; Vuister, G. W.; Zhu, G.; Pfeifer, J.; Bax, A. *J. Biomol. NMR* **1995**, *6*, 277−293.

(10) Zhu, G.; Bax, A. *J. Magn. Reson.* **1990**, *90*, 405−410.

(11) Garrett, D. S.; Powers, R.; Gronenborn, A. M.; Clore, G. M. *J. Magn. Reson.* **1991**, *95*, 214−220.

Table 1. NMR-Derived ψ Values (ψ_1,ψ_2) Determined from $\Gamma_{H\alpha C\alpha,HN}$ and $\Gamma_{H\alpha C\alpha,C'}$ Cross-Correlation Rates Either Individually[a] or in Combination[b] vs ψ Obtained from the X-ray Structure of CheY[21]

residue	$\psi_1(\Gamma_{H\alpha C\alpha,C'})$[a]	$\psi_2(\Gamma_{H\alpha C\alpha,C'})$[a]	$\psi_1(\Gamma_{H\alpha C\alpha,HN})$[a]	$\psi_2(\Gamma_{H\alpha C\alpha,HN})$[a]	ψ_1[b]	ψ_2[b]	ψ(X-ray)
K4	−112	−8	−101	−19	−12[c]		−17
E5	−122	2	−108	−12	−2		8
L6	113	127	96	144	101	139[d]	130
K7[e]			100	140	106	134	117
F8	89	151	97	143	93	147	143
V10	113	127	104	136	107	133	121
I20	−78	−42			−49		−49
N23	−86	−34	−76	−44	−36		−41
L25	−82	−38	−83	−37	−38		−45
K26	−80	−40	−78	−42	−41		−47
E27	−90	−30	−94	−26	−29		−30
N31	−111	−9	−110	−10	−10		−8
N32	92	148	87	153	89	151	79
V33	105	135	97	143	99	141	138
E34	80	160	76	164	78	162	160
E35	95	145	92	148	93	147	152
A36	90	150	89	151	89	151	149
E37	−108	−12	−108	−12	−12		−25
D41	−69	−51	−76	−44	−48		−46
A42	−76	−44	−68	−52	−47		−45
N44	−81	−39	−82	−38	−39		−48
K45	−78	−42	−75	−45	−43		−39
Q47	−101	−19	−91	−29	−22		−40
A48	−107	−13	−104	−16	−14		−15
Y51	102	138	89	151	92	148	147
F53	101	139	100	140	101	139	137
V54	116	124	97	143	102	138	135
I55	111	129	108	132	110	130	112
P61	88	152	82	158	83	157	163
M63	114	126	94	146	99	141	112
L66	−78	−42	−68	−52	−44		−41
E67	−85	−35	−77	−43	−38		−42
L68	−76	−44			−48		−48
L69	−71	−49			−65	−55	−50
K70	−84	−36	−88	−32	−34		−38
R73	−97	−23	−86	−34	−26		−33
A74	−110	−10	−108	−12	−10		−14
D75	113	127	90	150	97	143	122
A77	−98	−22	−92	−28	−24		−25
M78	−124	4	−108	−12	0		0
A80	−123	3	−115	−5	1		−8
P82	108	132	93	147	97	143	136
V83			107	133	117	123	116
M85	101	139	93	147	96	144	141
V86	105	135	96	144	99	141	129
T87	90	150	78	162	82	158	156
K92	−83	−37	−66	−54	−42		−51
E93	−90	−30	−93	−27	−29		−29
N94	−87	−33	−84	−36	−34		−48
I95	−78	−42			−47		−46
I96	−79	−41	−66	−54	−45		−46
A97	−80	−40	−76	−44	−42		−43
A98	−79	−41	−77	−43	−42		−47
A99	−78	−42	−77	−43	−42		−51
Q100	−90	−30	−85	−35	−32		−34
A101	−118	−2	−114	−6	−3		−2
A103	101	139	91	149	94	146	142
Y106	91	149	92	148	91	149	143
V107	97	143	85	155	89	151	136
V108	105	135	93	147	96	144	133
P110	100	140	85	155	90	150	152
F111	86	154	80	160	82	158	156
A113	−79	−41	−70	−50	−44		−42
L116	−80	−40	−71	−49	−43		−47
E117	−74	−46	−71	−49	−47		−48
K119	−78	−42	−73	−47	−43		−43
L120	−70	−50	−75	−45	−48		−53
N121	−83	−37	−84	−36	−36		−42
K122	−85	−35	−83	−37	−36		−47
I123	−74	−46	−75	−45	−46		−48
E125	−91	−29	−83	−37	−32		−46
L127	−116	−4	−105	−15	−7		2

[a] Only the ψ values consistent with those obtained by a combined fit of $\Gamma_{H\alpha C\alpha,HN}$ and $\Gamma_{H\alpha C\alpha,C'}$ cross-correlation rates are indicated. [b] Values of ψ calculated as described in the Materials and Methods. [c] For $-50° \leq \psi \leq 40°$ only a single ψ value is reported (see text and Figure 3b). [d] There are two possible ψ values consistent with the $\Gamma_{H\alpha C\alpha,HN}$ and $\Gamma_{H\alpha C\alpha,C'}$ cross-correlation rates. [e] Γ value close to an extrema in the Γ vs ψ profile. In this case an error in Γ can result in large errors in ψ, as described in the text. Values of ψ obtained from cross-correlation rates near the extrema are not included. Note that a good agreement between the X-ray derived values and ψ obtained when $\Gamma_{H\alpha C\alpha,HN}$ and $\Gamma_{H\alpha C\alpha,C'}$ are fit simultaneously is nevertheless obtained.

The experiment is based on the HN(CO)CA scheme that was published several years ago,[12] with the following transfer steps:

$$\mathrm{HN} \xrightarrow{J_{\mathrm{NH}}} {}^{15}\mathrm{N} \xrightarrow{J_{\mathrm{NC'}}} {}^{13}\mathrm{C'} \xrightarrow{J_{\mathrm{C'C\alpha}}} {}^{15}\mathrm{N}{}^{13}\mathrm{C}^{\alpha}\,(\mathrm{CT}\ t_1) \xrightarrow{J_{\mathrm{C'C\alpha}}} {}^{13}\mathrm{C'} \xrightarrow{J_{\mathrm{NC'}}} {}^{15}\mathrm{N}\,(\mathrm{CT}\ t_2) \xrightarrow{J_{\mathrm{NH}}} \mathrm{HN}\,(t_3) \quad (2)$$

where the term $^{15}N^{13}C^{\alpha}$ denotes double- and zero-quantum $^{15}N-{}^{13}C^{\alpha}$ coherences, CT t_i is a constant time acquisition period, and the couplings that are active during each transfer step are indicated above the arrows. At point a in the pulse scheme double- and zero-quantum $^{15}N-{}^{13}C^{\alpha}$ coherences are created and allowed to evolve for the period extending between points a and b in Figure 1. The sequence has been designed in this interval with a number of considerations in mind. First, cross-correlation between $^{13}C^{\alpha}-{}^{1}H^{\alpha}$ and $^{15}N-{}^{1}HN$ dipolar interactions must proceed for the complete period. This can be accomplished by ensuring that the relative signs of the dipolar Hamiltonians which give rise to the effect studied here are preserved,[6] since the cross-correlation rate is proportional to the product of the magnitudes of the individual Hamiltonians. Recalling that the operative dipolar Hamiltonians in the present case can be written as

$$H_1({}^{13}\mathrm{C}^{\alpha}-{}^{1}\mathrm{H}^{\alpha}) \propto \mathrm{C}^{\alpha}{}_z\mathrm{H}^{\alpha}{}_z$$

$$H_2({}^{15}\mathrm{N}-{}^{1}\mathrm{HN}) \propto \mathrm{N}_z\mathrm{H}^{\mathrm{N}}{}_z \quad (3)$$

where X_z denotes the z component of the spin angular momentum operator for spin X, it is clear that simultaneous application of $^{13}C^{\alpha}$ and ^{15}N or $^{13}C^{\alpha}$ and ^{1}HN pulses in the scheme of Figure 1 preserves cross-correlation during this interval.

A second important consideration is that the sensitivity of the experiment can be improved significantly by ensuring that net chemical shift evolution of only one of the two participating spins in the double-/zero-quantum coherence occurs during the constant time interval between points a and b.[6] Unlike the original scheme where separate double- and zero-quantum spectra are recorded,[4] double- and zero-quantum states are interchanged in the present experiment so that only the chemical shift of the $^{13}C^{\alpha}$ nucleus is measured during t_1. This is analogous to refocusing of the ^{1}H chemical shift in t_1 during recording of a $^{1}H-X$ HMQC spectrum.[13,14] Most important, a gain in sensitivity of a factor of 2 for each cross-peak is noted relative to the situation where correlations arising from both double- and zero-quantum states are recorded during t_1. The factor of 2 sensitivity gain can be appreciated more fully by considering the relevant density elements that evolve during the constant time interval extending from a to b in Figure 1. At the end of the constant time period of total duration T_C, the density elements corresponding to the double- and zero-quantum $^{15}N-{}^{13}C^{\alpha}$ coherences are given by

$$\rho_{\mathrm{DQ}\alpha\alpha}(T_C) = \rho_{\mathrm{ZQ}\alpha\beta}(T_C)$$

$$\propto \exp(-i\omega_{\mathrm{DQ}\alpha\alpha}t_1/2)\exp(-\Gamma_{\mathrm{DQ}\alpha\alpha}T_C/2) \times \exp(-i\omega_{\mathrm{ZQ}\alpha\beta}t_1/2)\exp(-\Gamma_{\mathrm{ZQ}\alpha\beta}T_C/2)$$

$$= \exp[-i(\omega_{\mathrm{C}\alpha} + \pi J_{\mathrm{C}\alpha\mathrm{H}\alpha} + \pi J_{\mathrm{NH}})t_1] \times \exp[-(\Gamma_{\mathrm{DQ}\alpha\alpha} + \Gamma_{\mathrm{ZQ}\alpha\beta})T_C/2]$$

$$\rho_{\mathrm{DQ}\alpha\beta}(T_C) = \rho_{\mathrm{ZQ}\alpha\alpha}(T_C)$$

$$\propto \exp(-i\omega_{\mathrm{DQ}\alpha\beta}t_1/2)\exp(-\Gamma_{\mathrm{DQ}\alpha\beta}T_C/2) \times \exp(-i\omega_{\mathrm{ZQ}\alpha\alpha}t_1/2)\exp(-\Gamma_{\mathrm{ZQ}\alpha\alpha}T_C/2)$$

$$= \exp[-i(\omega_{\mathrm{C}\alpha} + \pi J_{\mathrm{C}\alpha\mathrm{H}\alpha} - \pi J_{\mathrm{NH}})t_1] \times \exp[-(\Gamma_{\mathrm{DQ}\alpha\beta} + \Gamma_{\mathrm{ZQ}\alpha\alpha})T_C/2] \quad (4)$$

$$\rho_{\mathrm{DQ}\beta\alpha}(T_C) = \rho_{\mathrm{ZQ}\beta\beta}(T_C)$$

$$\propto \exp(-i\omega_{\mathrm{DQ}\beta\alpha}t_1/2)\exp(-\Gamma_{\mathrm{DQ}\beta\alpha}T_C/2) \times \exp(-i\omega_{\mathrm{ZQ}\beta\beta}t_1/2)\exp(-\Gamma_{\mathrm{ZQ}\beta\beta}T_C/2)$$

$$= \exp[-i(\omega_{\mathrm{C}\alpha} - \pi J_{\mathrm{C}\alpha\mathrm{H}\alpha} + \pi J_{\mathrm{NH}})t_1] \times \exp[-(\Gamma_{\mathrm{DQ}\beta\alpha} + \Gamma_{\mathrm{ZQ}\beta\beta})T_C/2]$$

$$\rho_{\mathrm{DQ}\beta\beta}(T_C) = \rho_{\mathrm{ZQ}\beta\alpha}(T_C)$$

$$\propto \exp(-i\omega_{\mathrm{DQ}\beta\beta}t_1/2)\exp(-\Gamma_{\mathrm{DQ}\beta\beta}T_C/2) \times \exp(-i\omega_{\mathrm{ZQ}\beta\alpha}t_1/2)\exp(-\Gamma_{\mathrm{ZQ}\beta\alpha}T_C/2)$$

$$= \exp[-i(\omega_{\mathrm{C}\alpha} - \pi J_{\mathrm{C}\alpha\mathrm{H}\alpha} - \pi J_{\mathrm{NH}})t_1] \times \exp[-(\Gamma_{\mathrm{DQ}\beta\beta} + \Gamma_{\mathrm{ZQ}\beta\alpha})T_C/2]$$

where $\omega_{C\alpha}$ is the Larmor frequency of the $^{13}C^{\alpha}$ spin, $\rho_{\mathrm{MQ}ij}$ is a density matrix element corresponding to a double- (M = D) or zero-quantum (M = Z) transition with the spin states (α,β) of the H^{α} and HN spins given by i and j, respectively, and $\Gamma_{\mathrm{MQ}ij}$ is the relaxation rate of the MQij coherence. Since averaging of double- and zero-quantum components occurs during the T_C interval (for example, interchange of $DQ_{\alpha\alpha}$ and $ZQ_{\alpha\beta}$), the sensitivity of the experiment is doubled relative to the original scheme where the evolution of each of the eight density elements listed in eq 4 occurs at a unique frequency.

Additional improvements in the sensitivity of the experiment come about by eliminating evolution from passive scalar couplings which are operative during the T_C constant time interval. One solution to this problem in the case of evolution from $^{13}C^{\alpha}-{}^{13}C^{\beta}$ couplings is to set $T_C = 1/J_{C\alpha C\beta}$, so that evolution due to $J_{C\alpha C\beta}$ does not decrease the intensity of the signal.[15,16] Unfortunately, the efficient transverse relaxation of double- (DQ) and zero-quantum (ZQ) elements during this lengthy delay limits this approach to applications involving small proteins. Moreover, for many systems, a value of $T_C = 1/J_{C\alpha C\beta}$ is longer than optimal for measurement of cross-correlation rates. For example, in applications to ubiquitin (correlation time ≈ 4 ns), a T_C value of 24 ms has been employed. For studies of larger proteins where the maximal cross-correlation rate (and transverse decay) is increased a value of $T_C = 24$ ms may well result in poor signal-to-noise and in some cases fast relaxing multiplet components may completely disappear. It may well be beneficial, therefore, to decrease T_C in proportion to the increase in size of the protein studied, recognizing however that a minimum acquisition time of at least 10 ms is necessary for adequate resolution in the $^{13}C^{\alpha}$ dimension. With this in mind we prefer, therefore, to use a constant time interval where $^{13}C-{}^{13}C$ coupling evolution is refocused in a manner which is independent of the choice of T_C.[6] This is accomplished by

(12) Bax, A.; Ikura, M. *J. Biomol. NMR* **1991**, *1*, 99−104.

(13) Bax, A.; Griffey, R. H.; Hawkings, B. L. *J. Magn. Reson.* **1983**, *55*, 301−315.

(14) Mueller, L. *J. Am. Chem. Soc.* **1979**, *101*, 4481−4484.

(15) Vuister, G. W.; Bax, A. *J. Magn. Reson.* **1992**, *98*, 428−435.

(16) Santoro, J.; King, G. C. *J. Magn. Reson.* **1992**, *97*, 202−207.

applying *nonselective* carbon refocusing pulses between periods A and B and between periods C and D so that evolution from $^{13}C^{\alpha}-^{13}C^{\beta}$ scalar coupling precedes for the complete A + B and C + D intervals. In contrast, a $^{13}C^{\alpha}$-*selective* refocusing pulse (REBURP[17]) is applied at the midpoint of the T_C period so that net coupling evolution over the complete constant time interval does not occur. The refocusing bandwidth of the 2-ms selective REBURP pulse used has been described previously.[6] In cases where a lack of selectivity of the refocusing pulse is an issue, the complete EXORCYCLE of the pulse[18] ensures that only the sensitivity of the correlations and not the accuracy of the cross-correlation relaxation rate is affected. Where $^{13}C^{\alpha}$ and $^{13}C^{\beta}$ shifts lie within the bandwidth of the selective pulse (some Ser residues, for example), the intensity of cross-peaks can vary considerably in a manner dependent on the value of T_C used in the experiment.

During the T_C period evolution also arises from one bond $^{15}N-^{13}C^{\alpha}$ passive couplings, $^1J_{NC\alpha}$, involving both ^{15}N and $^{13}C^{\alpha}$ components of double- and zero-quantum coherences that evolve during this interval. The sequence of Figure 1 refocuses modulation from these couplings so that net evolution does not occur. It is noteworthy that in the original pulse scheme[4] the signal is modulated according to $\cos^2(\pi^1J_{NC\alpha}T_C)\cos(\pi J_{C\alpha C\beta}T_C)$, while in the case of the experiment of Figure 1, modulation according to $\cos(\pi J_{NC'}t_1)$ occurs. The sensitivity gain of the present experiment relative to the initial scheme[4] that arises from evolution/refocusing of these couplings is given by

$$G = [\sin(\pi J_{NC'}t_{1,max})/(\pi J_{NC'}t_{1,max})]/[\cos^2(\pi^1J_{NC\alpha}T_C)\times \cos(\pi J_{C\alpha C\beta}T_C)] \quad (5)$$

assuming that $t_{1,max}$ is sufficiently short so that multiplet components arising from $J_{NC'}$ are unresolved. For T_C and $t_{1,max}$ values of 26 ms, $^1J_{NC\alpha} = 11$ Hz, $J_{NC'} = 15$ Hz, and $G = 2$.

A drawback of the present experiment relative to the $^{13}C^{\alpha}-^1H^{\alpha}$ dipolar/$^{13}C'$ CSA cross-correlation scheme[5,6] is that four rather than two cross-peaks are obtained for each correlation, resulting in a decrease in both sensitivity and resolution. As discussed below and in detail elsewhere,[4] extraction of cross-correlated relaxation rates from the present data is predicated on the measurement of accurate intensities for each of the four lines (see below) of the multiplet derived from the coherences indicated in eq 4. This can be difficult for the two inner multiplet lines with components separated by only $J_{C\alpha H\alpha} + J_{NH} \approx 50$ Hz ($J_{NH} < 0$). Fortunately, it is possible to improve the resolution 2-fold and eliminate this problem by separating multiplet components derived from α and β HN spin states.

The approach that has been used to achieve this separation follows from earlier work of Yang and Nagayama[7] and more recently Sorensen et al.[8] Two 3D data sets are recorded where the multiplet components modulated by J_{NH} are either in-phase or anti-phase. Postacquisition addition or subtraction of the data generates separate spectra where cross-peaks are shifted either upfield or downfield by $J_{NH}/2$ Hz. This method is implemented in the present pulse scheme by recording separate data sets with $E = t_2/2 + 1/(4J_{NH})$ and $F = T_N/2 - 1/(4J_{NH})$ for the first spectrum and by incrementing each of ϕ_4, ϕ_5, and ϕ_6 by 90° and setting $E = t_2/2$ and $F = T_N/2$ for the second. Thus, with the first line of the phase cycle in the legend to Figure 1, the signal of interest is modulated according to $\cos(\omega_{C\alpha}t_1)\cos(\pi J_{C\alpha H\alpha}t_1)\cos(\pi J_{NH}t_1)$ for the first data set and by $\sin(\omega_{C\alpha}t_1)\cos(\pi J_{C\alpha H\alpha}t_1)\sin(\pi J_{NH}t_1)$ in the second. Addition and subtraction of the data (and associated F_1 quadrature components) gives rise to spectra with cross-peaks at F_1 frequencies of $\omega_{C\alpha} - \pi J_{C\alpha H\alpha} - \pi J_{NH}$, $\omega_{C\alpha} + \pi J_{C\alpha H\alpha} - \pi J_{NH}$ (data set 1) and $\omega_{C\alpha} - \pi J_{C\alpha H\alpha} + \pi J_{NH}$, $\omega_{C\alpha} + \pi J_{C\alpha H\alpha} + \pi J_{NH}$ (data set 2). Finally, it is important to note that immediately after the $^{13}C^{\alpha}$ and ^{15}N pulses at point b in Figure 1 the coherences of relevance are given by $N_ZC^{\alpha}{}_ZC'_Z$ and $N_ZC^{\alpha}{}_ZC'{}_ZH^N{}_Z$ for each of the two data sets. During the period of duration $2\tau_d$ that immediately follows the T_C interval, the signal arising from $N_ZC^{\alpha}{}_ZC'{}_ZH^N{}_Z$ decays more rapidly than the corresponding signal from $N_ZC^{\alpha}{}_ZC'_Z$ due to HN spin flips. Therefore, prior to data processing, the second data set is multiplied by $\exp(R_{1sel}2\tau_d)$, where R_{1sel} is the average selective T_1 spin flip rate for the HN protons. In the case of ubiquitin and CheY (see below), multiplicative factors of 1.04 and 1.08 were used.

The above discussion assumes that the excitation profile of the HN-selective pulse in Figure 1 results in complete inversion of all HN spins while leaving H^{α} spins unperturbed. In the case of outlying HN chemical shifts incomplete inversion leads to an additional set of (very small) doublets in each data set with frequencies of $\omega_{C\alpha} \pm \pi J_{C\alpha H\alpha}$. On the other hand, if H^{α} spins are perturbed by the pulse, cross-peaks are observed at $F_1 = \{\omega_{C\alpha} - \pi J_{C\alpha H\alpha} - \pi J_{NH}, \omega_{C\alpha} + \pi J_{C\alpha H\alpha} - \pi J_{NH}, \omega_{C\alpha} - \pi J_{NH}\}$ and at $\{\omega_{C\alpha} - \pi J_{C\alpha H\alpha} + \pi J_{NH}, \omega_{C\alpha} + \pi J_{C\alpha H\alpha} + \pi J_{NH}, \omega_{C\alpha} + \pi J_{NH}\}$ in data sets 1 and 2, respectively. The additional correlations at $F_1 = \omega_{C\alpha} \pm \pi J_{NH}$, arising from pulse imperfections, are much smaller than the other cross-peaks. It is noteworthy that, for a 2.3-ms HN-selective pulse with the REBURP[17] profile centered at 8.8 ppm, these extra correlations are observed for residues with H^{α} shifts greater than approximately 5.8 ppm or HN shifts less than 7 ppm or greater than 10.6 ppm (500-MHz ^1H frequency).

Measurement of $\Gamma_{H\alpha C\alpha,HN}$ from Cross-Peak Intensities. The value of $\Gamma_{H\alpha C\alpha,HN}$ can be obtained in a straightforward manner from the ratio

$$R = (I_{DQ\alpha\beta+ZQ\alpha\alpha}I_{DQ\beta\alpha+ZQ\beta\beta})/(I_{DQ\alpha\alpha+ZQ\alpha\beta}I_{DQ\beta\beta+ZQ\beta\alpha}) \quad (6)$$

where $I_{DQ\alpha\beta+ZQ\alpha\alpha}$ ($I_{DQ\alpha\alpha+ZQ\alpha\beta}$) and $I_{DQ\beta\beta+ZQ\beta\alpha}$ ($I_{DQ\beta\alpha+ZQ\beta\beta}$) are the intensities of the downfield and upfield doublet components in data set 1 (2), obtained as described above, and the $DQ_{\alpha\beta} + ZQ_{\alpha\alpha}$ ($DQ_{\beta\alpha} + ZQ_{\beta\beta}$) component is the most downfield (upfield) of the four. In this regard it is important to remember that the signs of J_{NH} and $J_{C\alpha H\alpha}$ are opposite. Using the results of eq 4 and of the Appendix, R can be rewritten as

$$R = \exp\{(\Gamma_{H\alpha C\alpha,HN} + \Gamma_{H\alpha N,HC\alpha})4T_C\} \quad (7)$$

where $\Gamma_{H\alpha N,HC\alpha}$ is the relaxation term arising from cross-correlation between $^1H^{\alpha}-^{15}N$ and $^1HN-^{13}C^{\alpha}$ dipolar interactions. Calculations show that the maximum $\Gamma_{H\alpha N,HC\alpha}$ value is less than 0.5% of the maximum of $\Gamma_{H\alpha C\alpha,HN}$ and to good approximation, therefore, $\Gamma_{H\alpha N,HC\alpha}$ can be neglected. Thus

$$\Gamma_{H\alpha C\alpha,HN} = (0.25/T_C)\ln(R) = \gamma_H\gamma_N r_{HN}^{-3}\gamma_H\gamma_C r_{HC}^{-3}(h/2\pi)^2[(3\cos^2\theta - 1)/5]\tau_C \quad (8)$$

where γ_i is the gyromagnetic ratio of spin i ($\gamma_N < 0$), r_{ij} is the internuclear distance between spins i and j, θ is the angle between the $^1HN-^{15}N$ and $^1H^{\alpha}-^{13}C^{\alpha}$ internuclear vectors, and τ_C is the correlation time of the assumed rigid and isotropically tumbling molecule.[4,19] The value of $\cos\theta$ can be related to ψ

(17) Geen, H.; Freeman, R. *J. Magn. Reson.* **1991**, *93*, 93−141.
(18) Bodenhausen, G.; Freeman, R.; Turner, D. L. *J. Magn. Reson.* **1977**, *27*, 511−514.
(19) A factor of 2 error in eq 3 of ref 4 has been corrected.

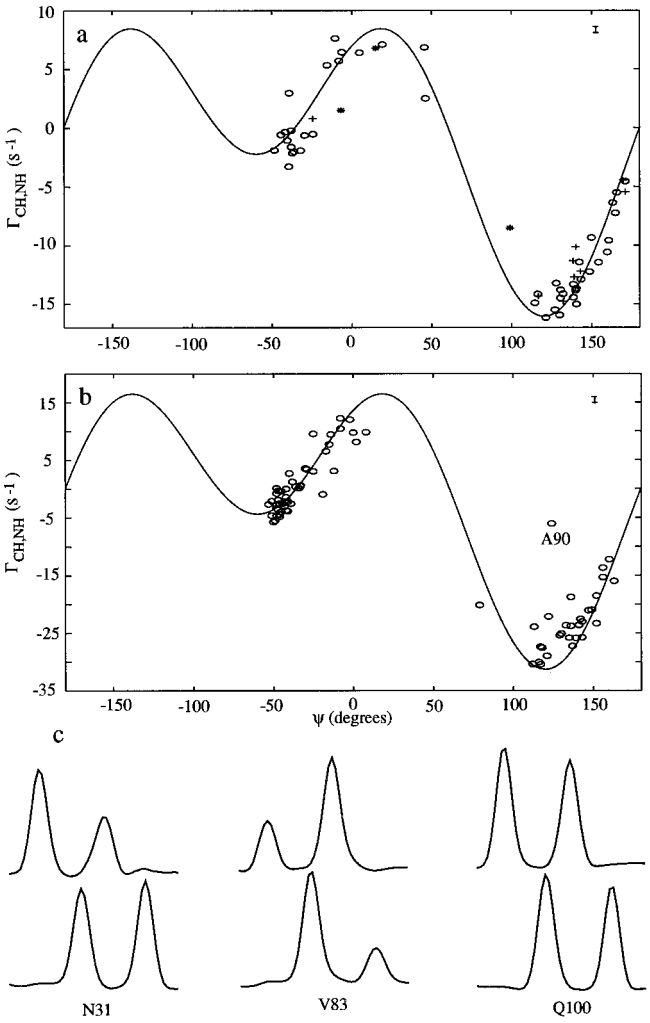

Figure 2. Correlation between calculated and experimental values of $\Gamma_{H\alpha C\alpha,HN}$ for ubiquitin (a) and CheY (b). Average errors are shown by the vertical bars in the upper right-hand corner. Curves were generated from eq 8 using standard bond lengths and angles with $r_{HN} = 1.02$ Å and $r_{HC} = 1.09$ Å. In panel a, residues for which the steady-state $^1H-^{15}N$ NOE (600 MHz) is greater than 0.7, between 0.6 and 0.7, and less than 0.6 are indicated by ○, +, and *, respectively.[24] (c) F_1 slices through Asn 31, Val 83, and Gln 100 illustrating the separation of the multiplet components according to the ^1HN spin state.

assuming planar peptide bond geometry according to

$$\cos\theta = 0.1628 + 0.8188\cos(\psi - 120°) \qquad (9)$$

as described by Reif et al.[4] We note that eq 8 is derived assuming that cross-correlation proceeds for the complete T_C period between points a and b in Figure 1. This presupposes that the cross-correlated spin relaxation rate is unaltered during the simultaneous application of $^{13}C^\alpha$- and ^1HN-selective REBURP[17] pulses. Simulations have established that this is a good assumption; $\Gamma_{H\alpha C\alpha,HN}$ is reduced by approximately 10% during the interval in which these pulses are applied (≈2 ms). We have therefore not corrected for this effect in the analysis of our data.

Protein Applications. Figure 2 illustrates the correlation between measured $\Gamma_{H\alpha C\alpha,HN}$ values for nonglycine residues in the proteins ubiquitin (a) and CheY (b) obtained using the scheme of Figure 1 and the predicted cross-correlation vs ψ profile generated from eqs 8 and 9. The values of ψ used in the Figure were obtained from the X-ray-derived structures of the molecules.[20,21] Correlation times of 4.0 ns (ubiquitin) and 7.8 ns (CheY) were used in the analysis of data based on ^{15}N relaxation measurements[22] and flexible terminal residues excluded (residues 72−74 for ubiquitin and 3 and 129 for CheY). It is noteworthy that the calculated $\Gamma_{H\alpha C\alpha,HN}$ vs ψ profile in Figure 2 is of opposite sign to the ones presented in Reif et al.[4] The difference arises from the fact that the negative sign of γ_N has been included in our calculations, and we have also noted that $J_{C\alpha H\alpha}$ and J_{NH} are of opposite sign in the analysis (see eqs 4 and 6). On average the correlation between predicted and measured $\Gamma_{H\alpha C\alpha,HN}$ values is quite good. In this regard, an outlier is observed for CheY (labeled A90 in Figure 2b), corresponding to $\Gamma_{H\alpha C\alpha,HN}$ for the $^1H^\alpha-^{13}C^\alpha$ and $^1HN-^{15}N$ dipole vectors of residues Ala 90 and Lys 91, respectively. The steady-state $^1H-^{15}N$ NOE for Lys 91 is low, 0.45, indicating that the amide of Lys 91 is flexible.[23] This underscores the importance of restricting the analysis to those residues with minimal internal dynamics, as established by ^{15}N relaxation studies. It is noteworthy that for Gln 62 and Leu 71 of ubiquitin where steady-state $^1H-^{15}N$ NOEs of 0.6 and 0.7, respectively, have been measured[24] differences of ≈10° between NMR and X-ray derived ψ values are observed (for residues Ile 61 and Val 70). In Figure 2a we have coded $\Gamma_{H\alpha C\alpha,HN}$ rates according to the $^1H-^{15}N$ NOE values of the $^1HN-^{15}N$ pair in question.

Figure 2c illustrates F_1 traces for residues Asn 31, Val 83, and Gln 100 of CheY. Upper and lower traces in Figure 2c are obtained from separate matrices generated by addition and subtraction of data sets as described above. Multiplet components in each trace are separated by $J_{C\alpha H\alpha}$, while components arising from the same residue are displaced by J_{NH} in the separate data sets. It is clear that excellent separation of components is achieved and that the resolution of doublet components in each data set is identical to the resolution in the $^{13}C^\alpha-^1H^\alpha$ dipolar/$^{13}C'$ CSA experiment.[5,6] It is worth emphasizing that the improvements in the dipole/dipole experiment described above, notably refocusing of passive $^1J_{NC\alpha}$ couplings and combining double- and zero-quantum correlations during the T_C interval, result in signal gains of a factor of 4 over the original experiment.[4] Nevertheless, in the scheme of Reif et al.,[4] separate double- and zero-quantum spectra are obtained allowing an independent measurement of ψ from each of the data sets. By averaging ψ values generated from each spectrum, it is thus possible to improve the precision by $\sqrt{2}$. Finally, the sensitivity of the scheme described in the present manuscript is approximately a factor of 2 lower than the dipolar/CSA-based sequence since four, rather than two, components are generated for each correlation.

The $\Gamma_{H\alpha C\alpha,HN}$ vs ψ profiles presented in Figure 2 illustrate that as many as four ψ values can be consistent with a single cross-correlation relaxation rate. With this limitation in mind we have analyzed $\Gamma_{H\alpha C\alpha,HN}$ and $\Gamma_{H\alpha C\alpha,C'}$ cross-correlation rates in the hope that a combination of these two measurements would limit the number of possible ψ values. Figure 3a shows $\Gamma_{H\alpha C\alpha,HN}$ (dashed line) and $\Gamma_{H\alpha C\alpha,C'}$ (solid line) profiles. By means of illustration, consider the case where values of 0.78 and -0.2 s^{-2} are measured for $\Gamma_{H\alpha C\alpha,HN} \times 10^{-9}/\tau_C$ and $\Gamma_{H\alpha C\alpha,C'}$

(20) Vijay-Kumar, S.; Bugg, C. E.; Cook, W. J. *J. Mol. Biol.* **1987**, *194*, 531−544.
(21) Stock, A. M.; Martinez-Hackert, E.; Rasmussen, B. F.; West, A. H.; Stock, J. B.; Ringe, D.; Petsko, G. A. *Biochemistry* **1994**, *32*, 13375−13380.
(22) Farrow, N. A.; Muhandiram, R.; Singer, A. U.; Pascal, S. M.; Kay, C. M.; Gish, G.; Shoelson, S. E.; Pawson, T.; Forman-Kay, J. D.; Kay, L. E. *Biochemistry* **1994**, *33*, 5984−6003.
(23) Moy, F. J.; Lowry, D. F.; Matsumura, P.; Dahlquist, F. W.; Krywko, J. E.; Domaille, P. J. *Biochemistry* **1994**, *33*, 10731−10742.
(24) Tjandra, N.; Feller, S. E.; Pastor, R. W.; Bax, A. *J. Am. Chem. Soc.* **1995**, *117*, 12562−12566.

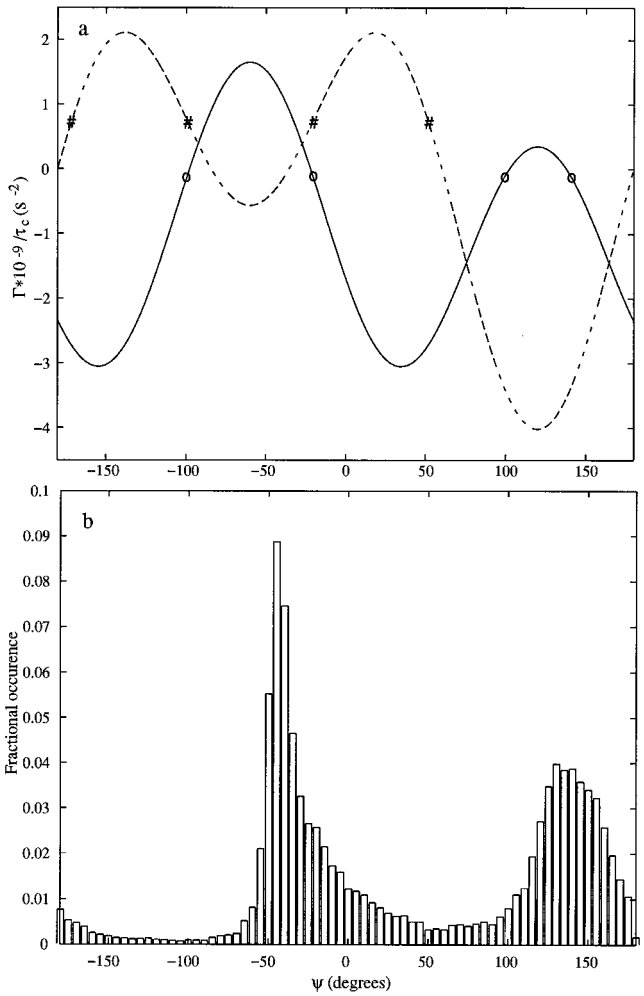

Figure 3. (a) Dependence of $\Gamma_{H\alpha C\alpha,HN}/\tau_c$ (- - -) and $\Gamma_{H\alpha C\alpha,C'}/\tau_c$ (—) on ψ. Multiple solutions for a given cross-correlation relaxation rate are illustrated by # and ○. (b) Distribution of ψ as established from high-resolution X-ray structures of 151 proteins.[25]

$\times 10^{-9}/\tau_C$, respectively. From the $\Gamma_{H\alpha C\alpha,HN}$ rate four ψ values are possible (−171°, −100°, −20°, 51°), while values of −100°, −20°, 98° and 142° are consistent with $\Gamma_{H\alpha C\alpha,C'} = -0.2$ s^{-2}. Thus, the combined use of $\Gamma_{H\alpha C\alpha,HN}$ and $\Gamma_{H\alpha C\alpha,C'}$ cross-correlation rates limits the possible ψ value to either −100° or −20°. To reduce the number of ψ values still further we have made use of an X-ray database comprised of 151 high-resolution structures[25] (1.8 Å or better). Figure 3b illustrates the ψ distribution observed in these 151 structures. Noting that ψ values ranging between −70° and −160° comprise in total less than 2.5% of the observed values suggests that to high probability potential ψ values in this range can be discarded. In addition, because both $\Gamma_{H\alpha C\alpha,C'}$ and $\Gamma_{H\alpha C\alpha,HN}$ profiles are symmetric about $\psi = -60°$ for $-180° \le \psi \le 60°$, values of ψ in the range from −50° to 40° can be uniquely determined with a high confidence level from the combination of these cross-correlation rates. On this basis, therefore, for the values of $\Gamma_{H\alpha C\alpha,HN}$ and $\Gamma_{H\alpha C\alpha,C'}$ discussed above, $\psi = -20°$ can be chosen with high probability.

Table 1 presents ψ values for CheY obtained by minimizing the differences between calculated and experimental $\Gamma_{H\alpha C\alpha,HN}$ and $\Gamma_{H\alpha C\alpha,C'}$ values (see Materials and Methods). In all cases a maximum of two possible values for ψ was obtained, while for helical regions a single ψ value was noted. Values of ψ obtained exclusively from either $\Gamma_{H\alpha C\alpha,HN}$ or $\Gamma_{H\alpha C\alpha,C'}$ (not both) and which are consistent with ψ calculated from the combined rates are also shown. In cases where Γ values are near extrema in the Γ vs ψ profile (see Figure 2) small errors in Γ can lead to large errors in ψ. For example in Figure 2 a number of cross-correlation rates are measured that lie below the calculated rate expected for ψ dihedral angles of ≈−50°. In these cases use of $\Gamma_{H\alpha C\alpha,HN}$ rates as the exclusive indicators of ψ would lead to incorrect values of ≈50°. This underscores the importance of using data from a number of different types of experiments to establish correct dihedral values. Values of ψ obtained from either $\Gamma_{H\alpha C\alpha,HN}$ or $\Gamma_{H\alpha C\alpha,C'}$ which are in significant error as a result of the above problem are not indicated in the table. It is noteworthy that, in all cases where such errors arise, use of both Γ rates results in ψ values which are in much better agreement with the X-ray angles.

Figure 4a illustrates the correlation between NMR and X-ray-derived ψ values for both ubiquitin and CheY in the case where only a single value of ψ is obtained ($-50° \le \psi \le 40°$). The pairwise root-mean-squared difference (rmsd) between ψ values in the range $-50° \le \psi \le 40°$ is 7°, with a maximum deviation of 17.3° for Gln 47 of CheY. It is interesting to note that the secondary structure in the immediate vicinity of Gln 47 is different in the X-ray[21] and NMR[23] structures, with an α-helix extending from residues 40−46 in the X-ray structure and from residues 40−48 in the NMR structure. Figure 4b shows the correlation between ψ values obtained from either $\Gamma_{H\alpha C\alpha,HN}$ or $\Gamma_{H\alpha C\alpha,C'}$ (not both) that are closest to the values generated when both Γ rates were fit simultaneously, as described in the Materials and Methods. Note that we have not excluded ψ values which have low probability (i.e., $-160° \le \psi \le -70°$, see Figure 3b). This comparison allows an assessment of errors in ψ resulting from the assumptions of a uniform C′ CSA tensor, constant HN and HC bond lengths, and the absence of internal dynamics (note that $\Gamma_{H\alpha C\alpha,HN}$ and $\Gamma_{H\alpha C\alpha,C'}$ can be affected differently by internal motions) that have been made in the analysis of the data. A pairwise rmsd between ψ values obtained using each method of 8° and 9.2° is obtained for ubiquitin and CheY, respectively, with maximal deviations of 18° (ubiquitin) and 23° (CheY). These differences are much larger than the errors in ψ estimated assuming that all of the error is derived from noise in the data sets (on average ±1−2°) and provide a much more reliable indication of the accuracy of the measurements.

Finally, we have also measured $\Gamma_{C\alpha C\beta,C'}$ rates in deuterated samples in the hopes of using both $\Gamma_{H\alpha C\alpha,C'}$ and $\Gamma_{C\alpha C\beta,C'}$ values to extract unique values of ψ. In this case the Γ vs ψ profiles are displaced by 120°, in principle allowing determination of a unique ψ value from the pair of measurements. In practice, however, the small values of $\Gamma_{C\alpha C\beta,C'}$ are difficult to measure

(25) Heringa, J.; Sommerfeldt, H.; Higgins, D.; Argos, P. *Comput. Appl. Biosci.* **1992**, *8*, 599−600.
(26) Shaka, A. J.; Keeler, J.; Frenkiel, T.; Freeman, R. *J. Magn. Reson.* **1983**, *52*, 335−338.
(27) Kay, L. E.; Ikura, M.; Tschudin, R.; Bax, A. *J. Magn. Reson.* **1990**, *89*, 496−514.
(28) Boyd, J.; Scoffe, N. *J. Magn. Reson.* **1989**, *85*, 406−413.
(29) Patt, S. L. *J. Magn. Reson.* **1992**, *96*, 94−102.
(30) Emsley, L.; Bodenhausen, G. *Chem. Phys. Lett.* **1987**, *165*, 469−476.
(31) McCoy, M. A.; Mueller, L. *J. Magn. Reson.* **1992**, *98*, 674−679.
(32) Marion, D.; Ikura, M.; Tschudin, R.; Bax, A. *J. Magn. Reson.* **1989**, *85*, 393−399.
(33) Kay, L. E.; Keifer, P.; Saarinen, T. *J. Am. Chem. Soc.* **1992**, *114*, 10663−10665.
(34) Schleucher, J.; Sattler, M.; Griesinger, C. *Angew. Chem., Int. Ed. Engl.* **1993**, *32*, 1489−1491.
(35) Kay, L. E. *J. Am. Chem. Soc.* **1993**, *115*, 2055−2056.

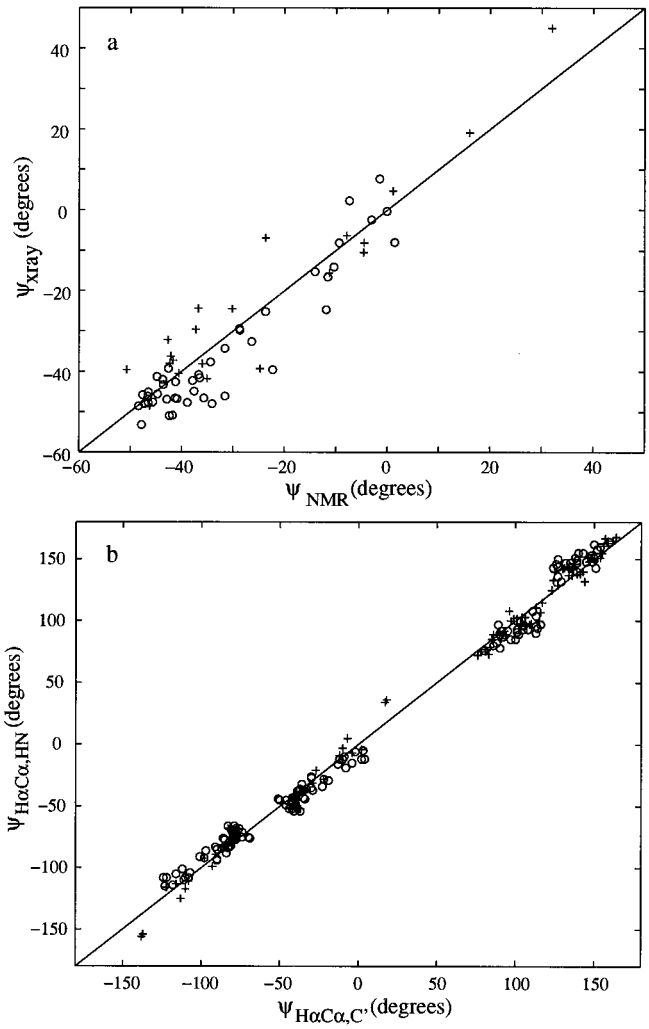

Figure 4. (a) Correlation between values of ψ determined from cross-correlation rates (ψ_{NMR}) and from the X-ray structures (ψ_{xray}) of ubiquitin[20] (+) and CheY[21] (○). ψ_{NMR} values in the range $-50° \leq \psi \leq 40°$ only are shown (see text). (b) Correlation between values of ψ obtained from either $\Gamma_{H\alpha C\alpha,HN}$ or $\Gamma_{H\alpha C\alpha,C'}$ cross-correlation rates (not both) that are closest to the values obtained when both rates are used in combination for ubiquitin (+) and CheY (○). For each residue, two potential values of ψ have been obtained; no attempt has been made to eliminate one of the possibilities on the basis of the database analysis discussed in the text.

accurately (approximate 10-fold reduction relative to $\Gamma_{H\alpha C\alpha,C'}$), at least at the field that we have used (500 MHz).

Concluding Remarks

A pulse sequence has been presented for measuring cross-correlation between dipolar interactions involving $^1H-^{13}C^\alpha$ and $^1HN-^{15}N$ dipoles of successive residues. The experiment has significantly improved sensitivity and resolution relative to a previous version.[4] In many cases, a combination of $\Gamma_{H\alpha C\alpha,HN}$ and $\Gamma_{H\alpha C\alpha,C'}$ cross-correlation relaxation rates decreases the number of possible ψ values from four to two, and for ψ values in the range $-50° \leq \psi \leq 40°$, a single value can be obtained with a high degree of confidence.

Acknowledgment. The authors are grateful to Professors J. Wand (SUNY, Buffalo) and Rick Dahlquist (Oregon) for kindly supplying $^{15}N,^{13}C$-labeled samples of ubiquitin and CheY and to Dr. Kevin Gardner (Toronto) for providing Figure 3b. This research was supported by the Natural Sciences and Engineering Research Council of Canada and the Medical Research Council of Canada. L.E.K. is an International Howard Hughes Research Scholar.

Appendix: Expression of Double-/Zero-Quantum Relaxation Rates in Terms of Individual Relaxation Contributions

In what follows we consider an isolated peptide fragment, $^1H^\alpha-^{13}C^\alpha-^{13}C'-^{15}N-^1HN$, and focus on the relaxation of the double- and zero-quantum $^{15}N-^{13}C^\alpha$ coherences during the interval extending from a to b in Figure 1 (duration T_C). The relaxation Hamiltonian, H, consists of $^1H^\alpha-^{13}C^\alpha$, $^1HN-^{15}N$, $^1H^\alpha-^{15}N$, and $^1HN-^{13}C^\alpha$ dipolar terms, as well as $^{13}C^\alpha$ and ^{15}N CSA contributions. (Note that $^{13}C^\alpha-^{13}C'$ and $^{13}C'-^{15}N$ dipolar terms have been neglected.) In principle, there are 15 cross-correlation terms that arise from the four dipolar and two CSA components of H. A straightforward, albeit lengthy, analysis establishes that of the 15 possible cross-correlation terms only 6 give nonzero net contributions to the relaxation of the individual double- and zero-quantum density elements according to

$$\Gamma_{DQ\alpha\alpha} = \Gamma_{ZQ\alpha\beta} = \Gamma_a + \Gamma_{H\alpha C\alpha,HN} + \Gamma_{H\alpha C\alpha,C\alpha} + \Gamma_{HN,C\alpha} + \Gamma_{H\alpha N,N} + \Gamma_{HC\alpha,N} + \Gamma_{H\alpha N,HC\alpha}$$

$$\Gamma_{DQ\beta\beta} = \Gamma_{ZQ\beta\alpha} = \Gamma_a + \Gamma_{H\alpha C\alpha,HN} - \Gamma_{H\alpha C\alpha,C\alpha} - \Gamma_{HN,C\alpha} - \Gamma_{H\alpha N,N} - \Gamma_{HC\alpha,N} + \Gamma_{H\alpha N,HC\alpha}$$

$$\Gamma_{DQ\alpha\beta} = \Gamma_{ZQ\alpha\alpha} = \Gamma_a - \Gamma_{H\alpha C\alpha,HN} + \Gamma_{H\alpha C\alpha,C\alpha} - \Gamma_{HN,C\alpha} + \Gamma_{H\alpha N,N} - \Gamma_{HC\alpha,N} - \Gamma_{H\alpha N,HC\alpha}$$

$$\Gamma_{DQ\beta\alpha} = \Gamma_{ZQ\beta\beta} = \Gamma_a - \Gamma_{H\alpha C\alpha,HN} - \Gamma_{H\alpha C\alpha,C\alpha} + \Gamma_{HN,C\alpha} - \Gamma_{H\alpha N,N} + \Gamma_{HC\alpha,N} - \Gamma_{H\alpha N,HC\alpha} \quad (10)$$

where Γ_a is the autorelaxation rate of each transition, $\Gamma_{ij,kl}$ is the cross-correlation rate arising from interference between dipolar interactions ij and kl, and $\Gamma_{ij,m}$ is the rate derived from cross-correlation between ij dipolar and m CSA interactions. In the subscripts defining the various interactions the $^1H^\alpha$ and ^1HN spins are denoted by Hα and H, respectively. Equation 7 is derived readily from eqs 6 and 10 by noting that $I_{DQij+ZQkl} = I(0)\exp[-\{(\Gamma_{DQij} + \Gamma_{ZQkl})/2\}T_C]$ in eq 6.

Supporting Information Available: Table comparing ψ values obtained from $\Gamma_{H\alpha C\alpha,HN}$ and $\Gamma_{H\alpha C\alpha,C'}$ cross-correlation relaxation rates with ψ values from the X-ray-derived structure of ubiquitin (2 pages, print/PDF). See any current masthead page for ordering information and Web access instructions.

JA981873K